Enrichment of organic nitrogen in fog residuals observed in the Italian Po Valley

Fredrik Mattsson[a,b], Almuth Neuberger[a,b], Liine Heikkinen[a,b], Yvette Gramlich[a,b,c], Marco Paglione[d], Matteo Rinaldi[d], Stefano Decesari[d], Paul Zieger[a,b], Ilona Riipinen[a,b], and Claudia Mohr[a,b,c,e]

[a]Department of Environmental Science, Stockholm University, Stockholm, Sweden
[b]Bolin Centre for Climate Research, Stockholm, Sweden
[c]PSI Center for Energy and Environmental Sciences, 5232 Villigen PSI, Switzerland
[d]Institute of Atmospheric Sciences and Climate, National Research Council, Bologna, Italy
[e]Department of Environmental Systems Science, ETH Zurich, Zürich, Switzerland

Correspondence: Claudia Mohr (claudia.mohr@psi.ch)

Abstract. While aerosol-cloud interactions have been extensively investigated, large knowledge gaps still exist. Atmospheric organic nitrogen (ON) species and their formation in the aqueous phase are potentially important due to their influence on aerosol optical and hygroscopic properties, and their adverse effects on human health. This study aimed to characterize the wintertime aerosol and fog chemical composition, with focus on the formation of ON, at a rural site in the Italian Po Valley.

5 Online chemical characterization of interstitial aerosol (non-activated particles) and fog residuals (dried fog droplets) were performed in parallel. Fog residuals were sampled using a Ground-based Counterflow Virtual Impactor (GCVI) inlet and analyzed by a Soot-Particle Aerosol Mass Spectrometer (SP-AMS), while the interstitial aerosol was characterized by a High-Resolution Time of Flight AMS (HR-TOF-AMS). Our results revealed an enhancement of nitrate (NO_3^-; 43.3% vs. 34.6%), ammonium (NH_4^+; 15.2% vs. 11.7%), and sulfate (SO_4^{2-}; 10.5% vs. 6.6%) in the fog residuals compared to the ambient

10 non-fog aerosol, while the organic aerosol (OA; 27.6% vs. 39.4%) and refractory black carbon (rBC; 2.3% vs. 6.3%) were less abundant. An enrichment of ON was observed in the fog, mainly consisting of $C_xH_yN_1^+$ ions, partly originating from amines. $C_xH_yN_2^+$ ions, fragments linked to imidazoles were over proportionally present in the fog, suggesting aqueous-phase formation, which was verified by proton nuclear magnetic resonance (1H-NMR) spectroscopy. This study demonstrates that fogs and clouds are potentially important sinks for gaseous nitrogen species and medium for aqueous production of nitrogen-

15 containing organic aerosol in the atmosphere.

1 Introduction

Aerosol particles have a significant impact on clouds and fogs, and a substantial indirect climate effect as a result (Szopa et al., 2021). The complex aerosol-cloud interactions are poorly constrained, especially on the micro-physical scale (Masson-Delmotte et al., 2021). The interactions of aerosol particles with fogs are largely analogous to the interactions with higher-altitude clouds. Fog droplets form by the condensation of water vapor onto aerosol particles, which act as cloud condensation nuclei (CCN). For radiation fog, this typically occurs overnight as the near-surface air cools and becomes saturated with respect to water vapor. The physical and chemical properties of the activated CCN influence the properties of the fog, such as the number and size of the fog droplets, the fog life cycle, as well as its effect on Earth's radiation budget (Jia et al., 2019; Duplessis et al., 2021).

Fog droplets can act as reactors for transforming both gases and aerosol particles through aqueous-phase reactions. For aerosol particles, this may result in an altered size, shape, and chemical composition of fog residuals as the fog dissipates (Ge et al., 2012; Seinfeld and Pandis, 2016). The organic aerosol (OA), which overall constitutes a significant mass fraction (20- 80%) of the atmospheric particulate matter (Zhang et al., 2007), has been shown to undergo chemical transformation in fog water (Mazzoleni et al., 2010; Ehrenhauser et al., 2012), with possible implications for aerosol reactivity and toxicity. Studying OA in the atmosphere poses significant challenges due to the vast range of different compounds (Goldstein and Galbally, 2007), as well as the continuous evolution as these compounds reside in the atmosphere (Jimenez et al., 2009). A large, often dominant fraction of this atmospheric OA is considered secondary organic aerosol (SOA) (Hallquist et al., 2009). Volatile organic compounds (VOCs) are SOA precursors, which can be emitted from both biogenic and anthropogenic sources. A major pathway for SOA formation is the partitioning of VOC-oxidation products into the particle phase. This process can be enhanced at high relative humidity for water-soluble compounds, where cloud/fog droplets or deliquesced aerosol particles act as a reactive media for new aqueous SOA (aqSOA) (Ervens et al., 2011).

While the formation mechanisms, precursors involved, and the necessary conditions for aqSOA production are poorly quantified, key reactions involved are recognized. Oxidation reactions occurring in the aqueous phase play a significant role in generating low-volatility products, such as dicarboxylic acids or keto acids (Ervens, 2015). Another pathway for certain VOCs, such as ethene and isoprene, to contribute to aqSOA is through oxidation leading to the formation of glyoxal ($C_2H_2O_2$) or methylglyoxal ($C_3H_4O_2$), which can generate low-volatility species by hydration or oligomerization reactions (Herrmann et al., 2015). For example, in the presence of amines or amino acids, dissolved glyoxal or methylglyoxal can form nitrogen-containing compounds, such as imidazole (De Haan et al., 2011; Ervens et al., 2011). These oxidized products result in an enhanced particulate mass, which can remain in the particle-phase after fog/cloud dissipation (Hallquist et al., 2009). Phenolic compounds, such as syringol and guaiacol have been found to form dimers or oligomers upon oxidation in the aqueous phase (Sun et al., 2010; Yu et al., 2014). Inorganic aerosol species also contribute to aqSOA. Nitrate (NO_3^-) is becoming more important as an aerosol component in many areas, due the reduction of other air pollutants (e.g. SO_2), or where high levels of excess NH_3 exist in the atmosphere (Bauer et al., 2007).

Atmospheric organic nitrogen (ON) are compounds ubiquitously observed in the atmosphere, and known to partake in
aqueous processes in fog and cloud droplets (Zhang and Anastasio, 2001; Laskin et al., 2015). However, their formation and
reactions involved are poorly understood. Gaseous and particulate ON represents about 30% of the total atmospheric nitrogen
and plays an important role in the terrestrial and aquatic nitrogen cycles (Cape et al., 2011; Jickells et al., 2013). Sources of
ON include emissions from vehicle exhaust, biomass burning, and agriculture (Rabaud et al., 2003; Cape et al., 2011), while
secondary formation may occur through VOC oxidation by the nitrate radical (Ng et al., 2017), and aqueous-phase reactions in
fog or clouds (Rehbein et al., 2011). ON includes a large range of compounds, of which amines, amino acids, amides, organo-
nitrates, nitro-compounds, and imidazoles (N-heterocyclic compounds) have been observed in fog or cloud water (Zhang et al.,
2012; Youn et al., 2015; Chen et al., 2018; Kim et al., 2019; Ge et al., 2024). ON can affect the climate, as it can influence
both optical (Laskin et al., 2015; Chen et al., 2018) and hygroscopic properties (Powelson et al., 2014) of the aerosol particles
– thereby influencing both the direct and indirect ways aerosol particles interact with radiation. Moreover, ON species, such as
amines and imidazoles, can have adverse effects on the environment and human health (Ge et al., 2011).

The chemical analysis of fog water and the interstitial aerosol particles has proven to be an efficient way to assess the
importance of aqSOA formation in cloud water (Gilardoni et al., 2016; Kim et al., 2019; Paglione et al., 2020). Within Europe,
the Po Valley stands out as an important measurement site, where the fog-processing of agricultural and industrial emissions
has been studied. With a population of approximately 20 million people, the Po Valley is a densely populated region, with one
of the highest levels of air pollution in Europe, recording annual mean $PM_{2.5}$ (particulate matter with a diameter of $2.5\,\mu m$
or smaller) concentrations between $20\text{-}30\,\mu g\,m^{-3}$ at several sites, well above the World Health Organization's recommended
guidelines of $5\,\mu g\,m^{-3}$ (EEA, 2020). The emission sources are mainly industrial, agricultural, and residential biomass burning
(Scotto et al., 2021). The valley is surrounded by the Alps in the north and west, and the Apennines in the south. This often
results in a stagnant atmosphere, a compact mixing layer, and weak wind speeds (Vecchi et al., 2019). As a result, long-lasting
episodes of high surface relative humidity (RH) and radiation fog events frequently occur during the colder winter months
(Giulianelli et al., 2014). These conditions prevent the dispersion of air pollution, which can lead to the formation and build-up
of secondary aerosol particles (Perrino et al., 2014). Over the past three decades, numerous research studies have delved into
these fog events. During this time, fog water pH has increased from about 5.5 to 6.5, likely due to the decreasing trends of NO_3^-
and sulfate (SO_4^{2-}). Simultaneously, the aerosol pH decreased from about 5 to 4, which was mainly contributed to ammonium
(NH_4^+), while decreasing RH and increasing temperature in the region also were major drivers (Paglione et al., 2021). The
physical properties of the Po Valley aerosol and fog droplets have been investigated by e.g. Noone et al. (1992), who found
that between 20 to 30% of the accumulation mode aerosol mass was scavenged by the fog. Biomass burning emissions have
a significant influence on the aerosol mass, especially during the cold months, and contribute to aqSOA formation (Gilardoni
et al., 2016; Paglione et al., 2020). Furthermore, it has been established that SOA dominates the OA mass in this region,
where biomass burning is a major contributor (30% - 80%) to the PM_1 mass, both to the primary OA and the SOA during
the winter months (Saarikoski et al., 2012; Paglione et al., 2020). ON has previously been observed in the Po Valley. For
example, Montero-Martínez et al. (2014) found a good linear correlation between water soluble ON and NO_3^-, NH_4^+ and SO_4^{2-}
ions, while biomass burning was proven to be a potentially significant night-time contributor to ON. Saarikoski et al. (2012)

identified a nitrogen-containing OA factor from positive matrix factorization (PMF). $C_xH_yN_1$ compounds comprised 14% of
this factor, which also showed a good linear correlation with NO_3^- and NH_4^+. The role of fog in ON formation and content of
aerosols in the Po Valley has not been investigated in detail to date.

There are many challenges involved in obtaining in-situ cloud measurements, as it typically requires an aircraft. By focusing
on fog, many of these restrictions can be avoided. The analysis of the Po Valley aerosol-fog interactions has so far been
restricted, along with studies performed elsewhere, to offline chemical analysis of fog water or aerosol chemical composition,
or to in-situ analysis of interstitial aerosol particles. In situ-measurements of fog droplet residuals are lacking, limiting our
understanding of aerosol-fog interactions.

In this study, the Po Valley fog was thoroughly investigated by performing online measurements of the ambient aerosol and
the fog residuals, as well as collecting fog water for offline analysis, as part of the Fog and Aerosol InteRAction Research Italy
(FAIRARI, Neuberger et al., 2024, in press) campaign 2021/2022. The composition of the ambient aerosol, interstitial aerosol,
and fog residuals was characterized using a Soot-Particle Aerosol Mass Spectrometer (SP-AMS) and a High-Resolution Time
of Flight Aerosol Mass Spectrometer (HR-TOF-AMS) in parallel, while fog water samples were studied offline using the SP-
AMS and a Proton Nuclear Magnetic Resonance (1H-NMR) spectroscopy. Previous studies performing online quantification of
ON are limited compared to other OA species. However, the findings from Kim et al. (2019), Ge et al. (2024), and Graeffe et al.
(2022) have shown that ON can be identified and quantified in the ambient aerosol. This work presents an effort to highlight
particulate ON existing in fog water and fog residuals.

2 Methods

2.1 The FAIRARI campaign

The Fog and Aerosol InteRAction Research Italy (FAIRARI) campaign was conducted between November 2021 and April
2022, and took place at San Pietro Capofiume (SPC) in the Po Valley, Italy (Neuberger et al., 2024, in press). The main goals
of the campaign were to study various properties of aerosol particles, fog droplets, and precursor gases, in order to better
understand aerosol-fog interactions. This study focuses on the period of February and March 2022, when the mobile aerosol-
cloud laboratory, a measurement container equipped with instrumentation to study aerosol particles and cloud/fog droplets,
was at SPC.

2.2 Measurement site

The SPC research station (44°39'15"N, 11°37'29"E) is a rural measurement site, located in the Po Valley, about 30 km north-
east of Bologna, Italy. Standard particle- and gas-phase, as well as meteorological parameters are monitored continuously at
the site, both by the Regional Agency for Prevention, Environment, and Energy of Emilia-Romagna (ARPAE-ER), and the
Italian National Research Council – Institute of Atmospheric Sciences and Climate (CNR-ISAC). Meteorological data, such as
temperature, RH, and wind speed were provided by CNR-ISAC. Since the 1980s, numerous field studies have been conducted

115   at SPC, focusing on aerosol physical and chemical processes in fog (Noone et al., 1992; Facchini et al., 1999; Gilardoni et al., 2014), OA and its sources (Gilardoni et al., 2016; Paglione et al., 2020), gas-phase chemistry (Cai et al., 2024), and new particle formation (Lampilahti et al., 2021).

2.3   The mobile aerosol-cloud laboratory

The mobile aerosol-cloud laboratory consists of a wide range of instruments for characterizing aerosol particles, fog, and the
120   meteorological conditions. The indoor temperature was controlled and set to 21 °C. For more details about the instrumental setup inside the aerosol-cloud laboratory, see Neuberger et al., (2024, in press). The laboratory had two inlets sampling in parallel (Fig. 1): a whole-air inlet (WAI) and a Ground-based Counterflow Virtual Impactor (GCVI; Brechtel Mfg. Inc., USA, Model 1205) inlet. The WAI sampled the total ambient aerosol with a flow of 99 lpm, of which 80 lpm was make-up flow. The inlet was heated to around 20 °C until 2022-02-19, when it was changed to 30 °C.

125   The sampling of dried fog droplets (fog residuals) was done using the GCVI inlet. For a more technical description of the GCVI inlet, see Shingler et al. (2012) and Karlsson et al. (2021). In brief, the working principle of the GCVI is that two opposing air flows (a sample flow and a dry, particle-free counterflow) separate particles depending on their inertia. First, the particles are accelerated onto the tip of the inlet by the wind tunnel. This concentrates the particles, resulting in an enrichment of the fog/cloud droplets compared to in the ambient air, which has to be corrected for. The interstitial aerosol is caught by
130   an opposing counter-flow, while large enough particles, i.e. fog or cloud droplets, continue traveling through the GCVI, and are simultaneously dried. The resulting dried fog droplets are referred to as fog residuals in this study. During the FAIRARI campaign, the lower cut size of the GCVI inlet was set to 7.7 μm aerodynamic diameter, the enrichment factor was 6.7, and the sample flow through the GCVI was kept at 15 lpm. It should be noted that we did not account for the droplet sampling efficiency of the GCVI (Shingler et al., 2012; Karlsson et al., 2021), the sampled fog residual masses therefore have to be considered
135   as an underestimate of the real ambient values. Visibility was measured by a sensor (Model 6400, Belfort Instrument, USA). Whenever the visibility was lower than 1 km, which follows the definition of fog by the World Meteorological Organization, the GCVI inlet was automatically activated, and simultaneously, a number of the instruments switched from measuring behind the WAI to behind the GCVI (Neuberger et al., 2024, in press).

    The total length of the sampling lines from the WAI and GCVI to the SP-AMS were 578 cm and 360 cm, respectively.
140   The sampling line from the WAI consisted of 380 cm 1/4 inch inner diameter (ID) stainless steel tubing and 198 cm black conductive 1/4 inch ID tubing, while the GCVI sampling line consisted of 305 cm 1/4 ID inch stainless steel tubing and 55 cm 1/4 ID black conductive tubing. Behind the 3-way switch (Fig. 1), the sample flow was 2 lpm, where the SP-AMS flow was 0.1 lpm. The aerosol was consistently dried to below 30% RH, using a 100 cm Nafion dryer model MD-700 (Perma Pure LLC, NJ, USA).

145   ### 2.4   Aerosol chemical composition measurements

The Soot-Particle Aerosol Mass Spectrometer (SP-AMS; Aerodyne Research Inc., USA) (Onasch et al., 2012) is a High-Resolution Time of Flight Aerosol Mass Spectrometer (HR-TOF-AMS) (DeCarlo et al., 2006), equipped with a laser vaporizer
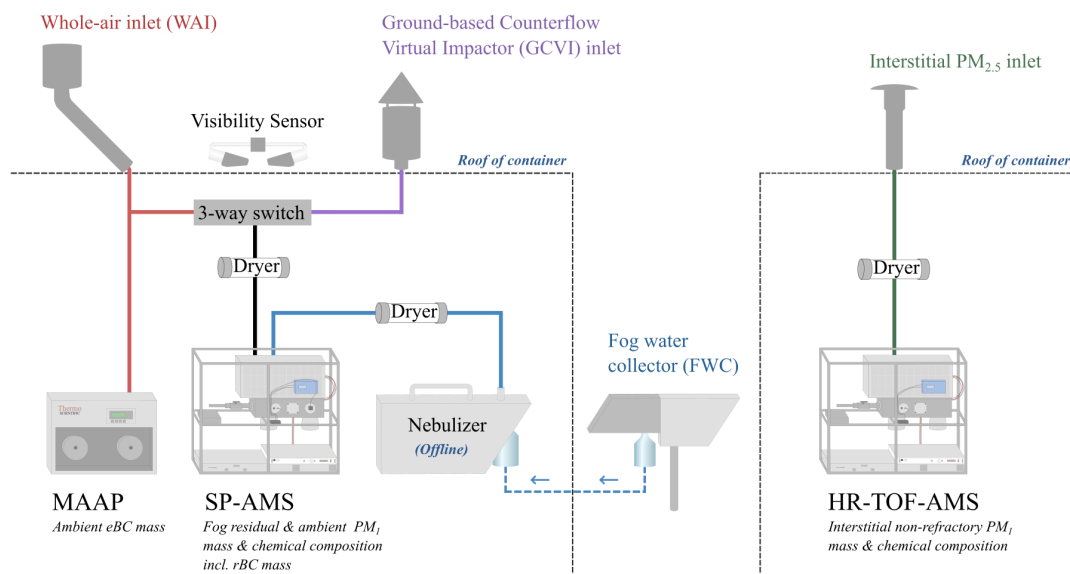
Figure 1. Schematic of the experimental set-up inside the two containers, including instruments relevant in this study. The two inlets in parallel, connected with a 3-way switch, allow selected instruments to change sampling inlet from the WAI to the GCVI during fog. The different colored lines represent how the instruments were connected during ambient aerosol sampling using the WAI (red), during fog events using GCVI inlet (purple), and the interstitial aerosol sampling (green). Offline fog water analysis was performed in laboratory (blue).

in addition to the tungsten vaporizer. It measures the size-resolved aerosol mass concentration of the non-refractory submicron particulate matter (NR-PM$_1$), which includes OA, NO$_3^-$, SO$_4^{2-}$, NH$_4^+$, and Cl$^-$, as well as refractory black carbon rBC. Aerosol

150 size distribution information is determined from the particles' time of flight using ePToF (efficient particle time-of-flight). Upon exiting the aerodynamic lens, the particles have a size-dependent velocity. The beam of particles hits a spinning chopper wheel with multiple slits. The time the particles need to go from an opening in the chopper to being acquired as several mass spectra in the mass spectrometer is used to determine the size of the particles (DeCarlo et al., 2006). Due to the additional laser vaporizer, based on the principle of the Single Particle Soot Photometer (SP2; Droplet Measurement Technology, USA, Stephens et al.,

155 2003), the quantification of rBC is achievable with the same instrument.

Throughout the study, the SP-AMS was alternating between three sampling modes; a single-vaporizer V-mode (30 minutes), a dual-vaporizer V-mode (30 minutes), and a single-vaporizer W-mode (15 minutes). In the single-vaporizer V-mode, the tungsten vaporizer is heated to 600 °C in order to flash-vaporize the NR-PM$_1$. The vaporized particle components are ionized, using 70 eV electron impact ionization, and continue into the extraction region of the mass spectrometer. The ions are sepa-

160 rated according to their mass to charge ratio (m/z), by following a V-shaped trajectory, first to the reflectron, and then back to the multichannel plate (MCP) detector. During dual-vaporizer mode, the rBC particles are vaporized using an intra-cavity Nd:YAG laser (1064 nm). In the single-vaporizer W-mode, once again, only the tungsten vaporizer is activated, however, here, the ions entering the mass spectrometer follow a W-shaped trajectory. The ions are initially directed into a hard mirror, which

makes the ions take a second flight to the reflectron before they reach the MCP detector. This provides a higher mass resolution
(m / Δm = 3500) compared to the V-mode (m / Δm = 2400) (DeCarlo et al., 2006).

All SP-AMS data were processed and analyzed using the AMS data analysis software packages SQUIRREL 1.66 and PIKA
1.26 (Sueper, 2024), together with Igor Pro 9 (Wavemetrics, USA). The data were recorded at a 1-minute resolution, which
was used during analysis. The ionization efficiency was calculated from calibrations using 300 nm ammonium nitrate particles.
For the rBC calibration, monodisperse rBC particles were created and nebulized using regal black mixed with milliQ water.
The resulting relative ionization efficiencies for ammonium, nitrate, organics, sulfate, chloride, and rBC were 3.4, 1, 1.4, 1.2,
1.3, and 0.2, respectively. The collection efficiency was calculated using the composition-dependent collection efficiency ap-
proach (Middlebrook et al., 2012), and was on average 0.54 throughout the measurement campaign. Due to an underestimated
ionization efficiency for the SP-AMS, the mass concentration measured by the SP-AMS had to be corrected (see Fig. S1). This
was done using data from a collocated HR-TOF-AMS provided by CNR-ISAC (from now on called the interstitial AMS; see
below for further details), which in turn was validated against offline ion-chromatography on parallel PM_1 filter samples. The
underestimation of ionization efficiency likely originated from a faulty flow settings in the callibration setup of a Differential
Mobility Particle Sizer (DMPS) used for the AMS calibration. The correction factor applied to all SP-AMS data was on average
0.51. All elemental ratios, such as oxygen-to-carbon (O:C) and nitrogen-to-carbon (N:C) were calculated using the improved
ambient (IA) method within PIKA 1.26 (Canagaratna et al., 2015). In order to quantify the ON ion categories used in this
study, $C_xH_yN_1^+$, $C_xH_yN_2^+$, and $C_xH_yO_1N_1^+$, the high resolution W-mode data were used during peak fitting. The W-mode
was set to scan up to m/z 106, which means that only ON ions within this range were included during the peak fitting.

In addition to the SP-AMS rBC measurements, aerosol light absorption was measured using a multi-angle absorption pho-
tometer (MAAP; Thermo Fisher Scientific, USA) (Petzold and Schönlinner, 2004), which was used to verify the rBC mass
concentration from the SP-AMS. The mass absorption cross-section (MAC_{BC}) of $6.6\,\mathrm{m^2\,g^{-1}}$ was used to estimate the equiv-
alent BC (eBC) mass concentration. During non-fog periods, both instruments measured behind the WAI.

Data from a second HR-ToF-AMS (interstitial AMS) were used to provide complementary information on the interstitial
aerosol (i.e., non-activated aerosol particles) chemical composition during fog events. The data from the interstitial AMS were
analysed following the same protocol as described above for the SP-AMS, but the instrument was installed in a different
container and sampled aerosol particles through a $PM_{2.5}$ inlet. Therefore, during fog events, this AMS sampled only the
interstitial (unactivated) particles, while fog droplets (activated particles) could not reach the sampling line because of the
smaller cut-off of the sampling head (Neuberger et al., 2024, in press). In addition, the aerosol liquid water content (ALWC) was
predicted using the aerosol inorganic species (K^+, Ca_2^+, Mg_2^+, Na^+, NO_3^-, SO_4^{2-}, NH_4^+, Cl^-) as inputs in ISORROPIA-II
model (Fountoukis and Nenes, 2007).

2.5   Offline analysis of fog water and PM_1 samples

Fog water was sampled at the SPC field station using a Fog Water Collector (FWC), described in more detail by Fuzzi et al.
(1997), and previously used in Paglione et al. (2021). Briefly, the FWC is an automated active string collector and sampling is
dictated automatically by a built in detector. The threshold value for fog has previously been validated with liquid water content

measurements by Fuzzi et al. (1997). The fog droplets entered the collector via an airflow of about $17\,\mathrm{m^3\,min^{-1}}$ created by
a fan placed in the back of the FWC. The fog droplets impacted on stainless-steel strings, which led the droplets into a glass
200 bottle via a funnel. After collection, the fog water samples were filtered through 47 mm quartz-fiber filters and kept frozen until
they were analyzed.

The offline analysis of the fog water samples took place in the laboratory, where each sample was nebulized using a Topas
ATM 228 Aerosol Generator (Topas GmbH, Dresden, Germany) and measured with a SP-AMS. The aerosol was dried with
a diffusion dryer, and the RH was kept below 20% throughout the experiments. In total, 9 fog water samples were collected
205 in February and March 2022. Each fog water sample was analyzed using this setup for at least one hour, while the SP-AMS
altered between the same three sampling modes as during the ambient and fog residual measurements. In order to be sure of no
contamination from either previous samples or the background, blank samples of pure milliQ water were measured for at least
10 minutes between each fog water sample. The measured signal from the blank samples was negligible. During the analysis
of the fog water samples, relatively large peaks were observed in the mass spectra at m/z 73, 143, 207, 221, and 281. These
210 peaks are likely artifacts from the conductive silicone tubing (Timko et al., 2009), and thus excluded from the analysis.

Sub-micron particles were also sampled on pre-washed and pre-baked quartz-fiber filters (PALL, 15 cm size) using a HiVol
sampler (TECORA, Italy), equipped with a PM_1 sampling head (Digitel Elektronik AG, Switzerland), using a nominal flow
of $500\,\mathrm{l\,min^{-1}}$, located at ground level (Neuberger et al., 2024, in press). The HiVol quartz-fiber samples were analyzed to
chemically characterize the water soluble organic carbon and to identify 1H-imidazole, for the first time at SPC, using proton
215 nuclear magnetic resonance (1H-NMR) spectroscopy following the method described by Decesari et al. (2024). This method
was also used to investigate the presence of 1H-imidazole in the fog water samples.

3 Results

3.1 Time series of aerosol species, meteorological parameters, and fog events

During February and March 2022 of the FAIRARI campaign, a total of 11 fog events (see Sect. 2.3 for the definition of a fog
220 event) were measured with the aforementioned setup. Figure 2 presents an overview of the measurements, where Fig. 2a shows
the aerosol mass concentration of the different aerosol species measured with the SP-AMS, with the fog events marked as gray
bars. Over the two months, the average ambient total PM_1 mass concentration was $13.5 \pm 9.1\,\mathrm{\mu g\,m^{-3}}$, which consisted of: OA
$= 5.3 \pm 3.0\,\mathrm{\mu g\,m^{-3}}$, $NO_3^- = 4.4 \pm 4.3\,\mathrm{\mu g\,m^{-3}}$, $SO_4^{2-} = 1.1 \pm 0.8\,\mathrm{\mu g\,m^{-3}}$, $NH_4^+ = 1.6 \pm 1.4\,\mathrm{\mu g\,m^{-3}}$, $Cl^- = 0.2 \pm 0.2\,\mathrm{\mu g\,m^{-3}}$,
and rBC $= 0.5 \pm 0.3\,\mathrm{\mu g\,m^{-3}}$. The total PM_1 mass concentration and the fractional composition were generally within the
225 range of previous studies from the Po Valley (Paglione et al., 2020; Scotto et al., 2021). Compared to previous winter-time
measurements performed specifically at SPC, the average PM_1 mass concentration and the contribution of OA (39.4%) were
on average lower, while the contributions from the inorganic species: $NO_3^- = 34.6\%$, $NH_4^+ = 11.7\%$, and $SO_4^{2-} = 6.6\%$ were
slightly elevated in the current study (Carbone et al., 2010; Gilardoni et al., 2014).

During fog, the SP-AMS automatically switched from the WAI to the GCVI in order to measure the fog residuals, which
230 on average consisted of: OA $= 27.6\%$, $NO_3^- = 43.3\%$, $NH_4^+ = 15.2\%$, $SO_4^{2-} = 10.5\%$, and rBC $= 2.3\%$. During the same

fog events, the average interstitial aerosol consisted of OA = 32.9%, NO_3^- = 37.1%, NH_4^+ = 14.1%, SO_4^{2-} = 4.6%, and BC = 10.6%. The mass scavenging efficiency (η, Eq. 1) was calculated using the average mass concentration of each chemical species before fog formation and the interstitial aerosol (Noone et al., 1992).

$$\eta = 1 - \frac{[X]_{\text{interstitial}}}{[X]_{\text{before fog}}} \tag{1}$$

235 OA and BC were associated with the lowest mass scavenging efficiencies, on average 49 and 36%, respectively. NO_3^-, NH_4^+, and SO_4^{2-} were more readily scavenged by the fog, with average η = 57, 59, and 57%, respectively. Relative to both interstitial and ambient aerosol, a higher contribution of ammonium nitrate and ammonium sulfate were observed in the fog residuals, while OA and rBC represented a lower fraction. These results align with what was expected; partly that the already existing, more hygroscopic, inorganic aerosol was preferred as CCN during the formation of the fog, and partly that ammonium nitrate
240 and ammonium sulfate are more readily taken up by the fog droplets.

Figure 2b shows the variations in the hourly mean temperature and RH. During the first fog and pollution intense period (February 16-22), the temperature was on average 8.8 °C and during the fog events 2.8 °C. In the second fog and pollution intense period (March 27-30), the average temperature was 11.7 °C, whereas during the fog events it was 5.3 °C. The first intense period showed a larger aerosol mass concentration, especially inorganic species, than the second period. Furthermore,
245 this aerosol mass consisted of more ON and a higher aerosol liquid water content (ALWC) (Fig. 2c). By performing a Spearman's rank correlation test, a moderate correlation was found between the non-fog ambient aerosol ON mass concentration and the ALWC (r_s = 0.44, p = 0.052).

3.2 Comparison of two pollution episodes intersected by fog

Figure 3 shows the chemical composition of the aerosol at different stages of two periods with reoccurring fog events (February
250 16-22 and March 27-30), investigated in more detail here. Of these two periods, the first had particularly high PM_1 loadings as compared to the second one - offering a good case study for comparing aerosol-fog interactions with varying levels of pollution. The first, more polluted, fog intensive period (February 16-22) was initiated by a stagnation of the atmosphere (Neuberger et al., 2024, in press), and consequent build-up of pollution starting on Feburary 17 (Fig. 3a). This build-up persisted until February 20, independently of the fog events occurring every night. The PM_1 mass consisted of mainly NO_3^-, OA, and NH_4^+, while rBC
255 and SO_4^{2-} stayed constant over this period. Starting from February 20, the wind intensified, resulting in a dissipation of the pollution. Both the ambient and the fog residual PM_1 mass were dominated by inorganic species, especially NO_3^- (Fig. 3b). The fraction of OA and rBC decreased in the fog residuals, while the NH_4^+, SO_4^{2-} and NO_3^- showed similar or slightly higher mass fractions in fog residuals compared to ambient.

In the second fog intensive episode (March 27-30), the ambient NO_3^- fraction was comparatively smaller than in the first
260 episode, while the ambient fraction of OA, SO_4^{2-}, and rBC was larger than in the first episode. The ambient fraction of NH_4^+ was similar in both episodes. The higher ambient ratio of OA to NO_3^- in the second pollution episode is however not reflected in the fog residual composition; this looks very similar to the composition of the residuals in the first pollution episode with relatively
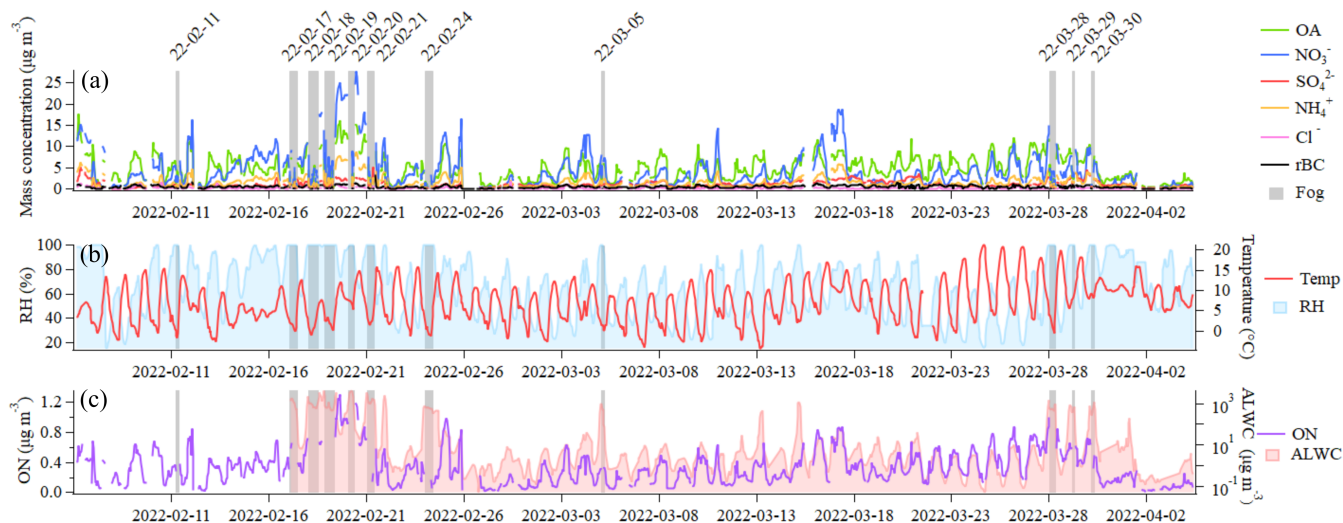
Figure 2. Overview of main parameters measured during the FAIRARI campaign from February to March, 2022. (a) shows the mass concentrations of aerosol chemical species recorded by the SP-AMS. The fog events are highlighted in gray shading, in which the SP-AMS measured the fog residuals behind the GCVI inlet. (b) shows the hourly mean temperature and relative humidity (RH). (c) shows the hourly averaged mass concentrations of the ON and the calculated ALWC.

higher nitrate contributions. During both episodes, the fog residuals were relatively enriched with inorganic components as compared to the ambient aerosols.

3.3 Chemical composition of ambient aerosol, interstitial aerosol, fog residuals, and fog water

We now compare in more detail the chemical composition of the average ambient aerosol before fog and after fog, and the interstitial aerosol to the fog residual and fog water composition (Fig. 4a). The ambient aerosol represents the average aerosol over the measurement campaign, excluding fog periods. Before and after fog is defined here as 1 - 2 hours before or after a fog event, while the interstitial (non-activated) aerosol is measured during the same fog events, by the interstitial AMS. Figure 4a reveals a scavenging of the inorganic species NO_3^-, SO_4^{2-}, and NH_4^+ from the interstitial mass fraction during fog. Simultaneously, these species are found enhanced in the fog residuals (68% of the PM_1 mass in fog), while most of rBC remained non-activated. The fractional compositions of the major chemical species before and after fog are relatively similar, showing that most of the particles taken up by the fog return to the particle-phase upon fog dissipation. Furthermore, before and after fog showed a higher contribution of NO_3^- compared to the average ambient non-fog periods, while fog water showed the highest fraction of total organic carbon.

Further investigating the organic mass fraction (Fig. 4a), according to its OA families (fragment elemental composition groups), similar composition was observed in the ambient, before, after, interstitial, and fog residuals, except for the nitrogen-containing OA families ($C_xH_yN_{1-2}^+$ and $C_xH_yO_1N_1^+$), which were enhanced in the fog residuals. This is also shown in Fig. 4b,
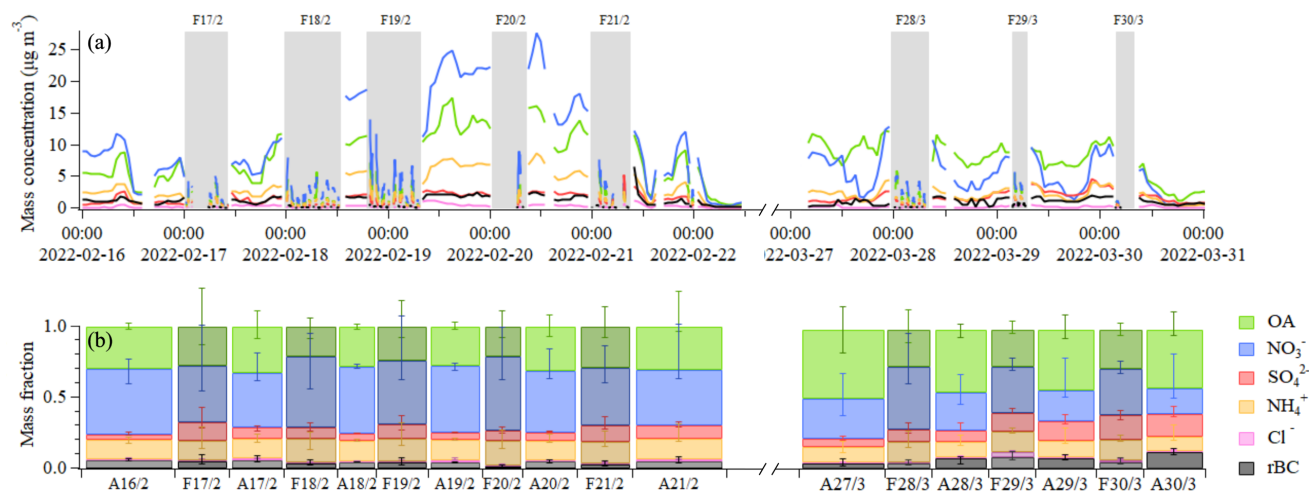
Figure 3. Fog intensive episodes between February 16-22 and March 27-30. (a) shows the aerosol mass time series from the SP-AMS. Fog events are indicated by gray bars. (b) shows the median mass fraction for each day, with the ambient (A) and fog residuals (F) separated. The width of each bar corresponds to the duration in (a), and the error bars represent the 75th and 25th percentile.
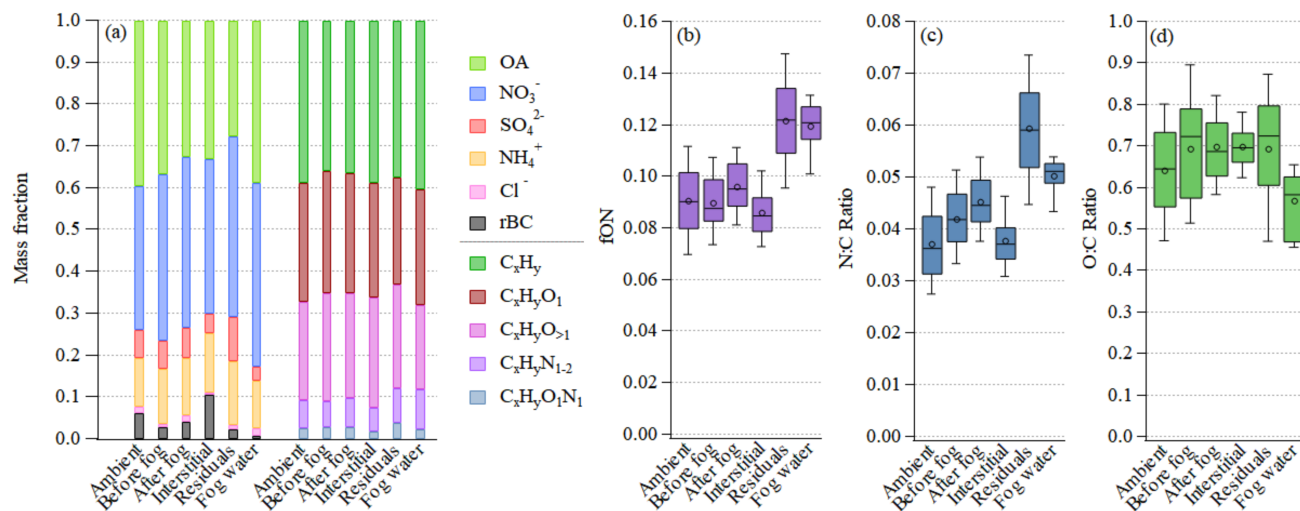
Figure 4. (a) Average mass fraction of the major aerosol species (left side) and the OA families (right side), box plots showing (b) the organic fraction of ON, (c) the N:C ratio, and (d) the O:C ratio. For all panels, the data are divided into 6 categories: ambient aerosol, before fog, after fog, interstitial, fog residuals, and fog water. For panels (b), (c), and (d), the whiskers above and below the boxes indicate the 90th and 10th percentile, the boxes indicate the 75th and 25th percentiles, the circles indicate the mean, and the lines indicate the median.

where the fON is the organic fraction of ON ions. The fog residuals, measured behind the GCVI, show a distinct enhancement

280 of ON (Fig. 4b), compared to the ambient aerosol. The nitrogen-to-carbon (N:C) ratio (Fig. 4c) was significantly higher in the fog residuals, highlighting elevated organic nitrogen that was present in the fog residuals compared to the ambient aerosol.

Similar to the fog residuals, the nebulized fog water samples showed an enhanced nitrogen-containing OA ($C_xH_yN_{1-2}^+$ and $C_xH_yO_1N_1^+$). Interestingly, this did not result in an equally high N:C ratio in the fog water, despite the high fraction of ON, indicating higher contributions of compounds with higher carbon numbers in the fog water as compared with the residuals.

285 This discrepancy is also reflected in the lower oxygen-to-carbon (O:C) ratio of the fog water, shown in Fig. 4d - in line with the organic mass fractions in Fig. 4a. In fact, the fog water samples contained a larger fraction of hydrocarbons ($C_xH_y^+$), mainly m/z 27 and 41, compared to the other categories. Simultaneously, the fraction of more oxidized OA ($C_xH_yO_{>1}^+$) was smaller compared to the other categories, resulting from a lower m/z 44 (CO_2^+) signal in the fog water compared to the fog residuals (Fig. S2). This could be, at least partly, due to the GCVI and WAI sampling inlets, where more volatile aerosol components

290 could evaporate and partition into the gas-phase due to the heating and drying, resulting in a higher O:C ratio for the fog residuals compared to fog water. However, the Po Valley fog water was expected to be relatively more oxidized. The fog water O:C ratio was previously estimated to 0.68 ± 0.08 at SPC (Gilardoni et al., 2016), which is similar to the current study's O:C ratio in the ambient, interstitial, and fog residuals. A previously observed O:C ratio in fog water from Fresno, California, was 0.42 ± 0.04, which is less oxidized than the Po Valley fog, but more similar to the Fresno pre- and post-fog (Kim et al., 2019).

295 At a polluted site in Kanpur, India, the fog water O:C ratio was estimated to $0.68 - 0.88$, which again is more in line with the current study's O:C ratio for the other categories (Chakraborty et al., 2016). Another hypothesis is that the larger fog droplets, sampled well by the FWC, have a different chemical composition compared to fog droplets sampled by the GCVI (smaller than $40\,\mu m$ diameter). Further research is needed on the discrepancies that arise from different fog/cloud measurement techniques.

3.4 Characterization of enhanced ON in fog residuals and fog water

300 The ON ions were divided into three OA families; $C_xH_yN_1^+$, $C_xH_yN_2^+$, and $C_xH_yO_1N_1^+$. The ON mass spectra observed in the fog water (Fig. 5b) and ambient aerosol (Fig. 5c) show similarities to ON mass spectra observed in wintertime Fresno, California (Kim et al., 2019; Ge et al., 2024). Both of these studies utilized an HR-TOF-AMS together with an atomizer for the offline analysis of fog water samples, similar to the fog water analysis in this study. The $C_xH_yN_1^+$ ions dominate all four ON mass spectra (Fig. 5), where a few of the observed peaks (e.g. CH_4N^+ and $C_2H_6N^+$) are tracer fragments of amines (Ge

305 et al., 2024). Most of the ON ions that appear in the fog residuals and fog water show similar relative abundance (Fig. S3), especially the lower m/z range ions with the highest signals (e.g. $C_1H_1N_1^+$ and $C_1H_1N_1O_1^+$). Over the full ON mass spectra, a high Pearson correlation coefficient was found between the fog residuals and fog water (r = 0.89). While most $C_xH_yO_1N_1^+$ ions constitute a larger fraction in the fog residuals, the $C_xH_yN_2^+$ ions show an opposite tendency.

$C_xH_yN_1^+$ ions were previously found as a major constituent in organic aerosol via source apportionment (Saarikoski et al.,

310 2012; Sun et al., 2011). During a spring-time field campaign at SPC in the Po Valley, Saarikoski et al. (2012) found a nitrogen-enriched OA (NOA) factor, where 14% of the factor was comprised of $C_xH_yN_1^+$ ions. This factor had a N:C ratio of 0.078, slightly higher than the fraction in the fog residuals in our study (Fig. 4c). They argue that this factor came from local traffic sources due to its diurnal trend and sharp decrease during the nocturnal surface layer break-up. This diurnal trend is neither
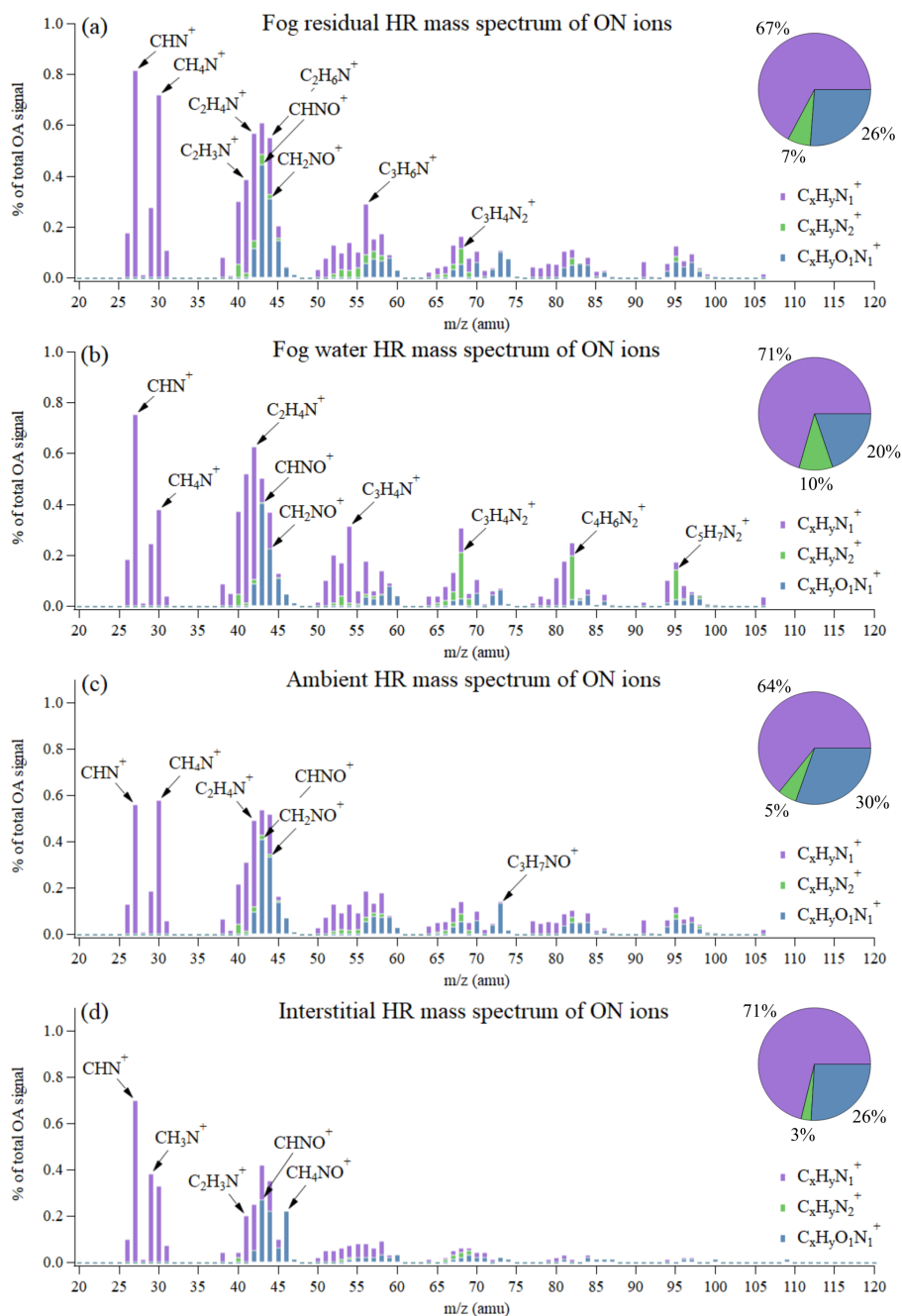
Figure 5. Average high resolution mass spectra of the nitrogen-containing organic ions presented as percentage of total OA signal in (a) fog residuals, (b) fog water, (c) ambient aerosol, and (d) interstitial aerosol. The pie charts show the fraction of each category ($C_xH_yN_1$, $C_xH_yN_2$, and $C_xH_yO_1N_1$).

observed in the N:C ratio nor for any ON compounds in this study. During non-fog conditions, the N:C ratio is in general high
during the day and low during the night, reaching its maximum around 14:00 local time. During the first fog and pollution
week, the N:C ratio shows less of a diurnal pattern, and stays at its maximum throughout the day.

A smaller fraction of the ON consisted of $C_xH_yN_2{}^+$ ions, ranging from 5% (ambient) to 10% (fog water). From the NIST
(National Institute of Standards and Technology Standard Reference) database on electron impact ionization mass spectra it
can be found that certain imidazoles have characteristic $C_xH_yN_2{}^+$ fragmentation peaks. The three $C_xH_yN_2{}^+$ peaks giving
the largest signal in the fog water mass spectra match with major signals for different imidazoles. Specifically, the $C_3H_4N_2{}^+$
peak at m/z 68 is likely 1H-Imidazole, while the $C_4H_6N_2{}^+$ peak at m/z 82 is likely related to 2-Methyl-1H-imidazole, and
$C_5H_7N_2{}^+$ at m/z 95 could be a fragment of 3,5-Dimethylpyrazole.

The presence and concentration of 1H-Imidazole were confirmed through 1H-NMR analysis conducted on the PM_1 filter
samples and fog water samples (Fig. 6). This compound produced two distinct singlets at 7.47 and 8.69 ppm of chemical shift
and was identified by comparison with a 1H-Imidazole standard under identical 1H-NMR experimental conditions (Fig. S4).
Notably, 1H-Imidazole was found in all fog water samples at relatively high levels, while only trace amounts were detected in
the PM_1 samples. This strongly suggests that the compound formed under aqueous conditions, possibly through the dissolution
of the gaseous fraction into fog droplets or water. Additionally, the concentrations obtained via 1H-NMR showed a reasonable
similarities with those measured by SP-AMS. Imidazole formation from aqSOA reactions is known to occur in the atmosphere
based on laboratory evidence (Herrmann et al., 2015). The first observation of imidazole in laboratory-generated aerosol
particles was done by Laskin et al. (2009), while the first in-situ observation of imidazole in the particle-phase was reported
by Teich et al. (2016). Recent experiments focusing on the characterization of ON in fog water have suggested the attribution
of AMS fragments to imidazoles (Kim et al., 2019; Ge et al., 2024), which were also found in the current study. However,
the formation of imidazole by aerosol-fog interactions has previously never been confirmed by a molecular-level analysis
integrated with online observation using aerosol mass spectrometry.

Previous laboratory studies have found evidence of aqueous-phase production of imidazoles from uptake of glyoxal with
amino acids (De Haan et al., 2009) and with ammonium sulfate (Galloway et al., 2009). By performing Pearson's correlation
coefficient (r) tests, no significant linear correlation was found between the imidazole fragments and typical glyoxal fragments
($C_2H_2O_2{}^+$, $C_2H_2{}^+$, $CH_2O_2{}^+$, Paglione et al., 2020) over the full measurement period in the ambient aerosol (r=0.38) and
the fog residuals (r=0.37). However, considering only the second fog intensive episode (March 27-30), the $C_xH_yN_2{}^+$ ions
were much more abundant in the ambient aerosol and fog residuals, and a linear correlation between imidazole fragments
and glyoxal fragments was found in both the ambient aerosol (r=0.65) and the fog residuals (r=0.70). This shows that during
the second foggy period, the $C_xH_yN_2{}^+$ ions increased in mass concentration in the fog residuals, and that they persisted in
the aerosol after fog dissipation. Meanwhile, a good linear correlations were found between the $C_xH_yN_1{}^+$ ions and glyoxal
fragments over the campaign (ambient r=0.80 and fog residuals r=0.84).

Due to the low volatility of imidazoles, they are expected to remain in the particle phase after droplet evaporation in the
different inlets and drying of the aerosol. A possible explanation why the $C_xH_yN_2{}^+$ ions were reduced in the online measure-
ments, compared to fog water samples, could be that they were more concentrated in evaporating larger fog droplets. Large

droplets were sampled with a high efficiency by the fog water sampler. The FWC had a 50% collection efficiency for each indi-
vidual string at approximately 3 mm droplet radius (Paglione et al., 2021), thus sampling larger droplets much more efficiently
compared to the GCVI, which does not sample droplets larger than approximately 40 μm (Shingler et al., 2012).
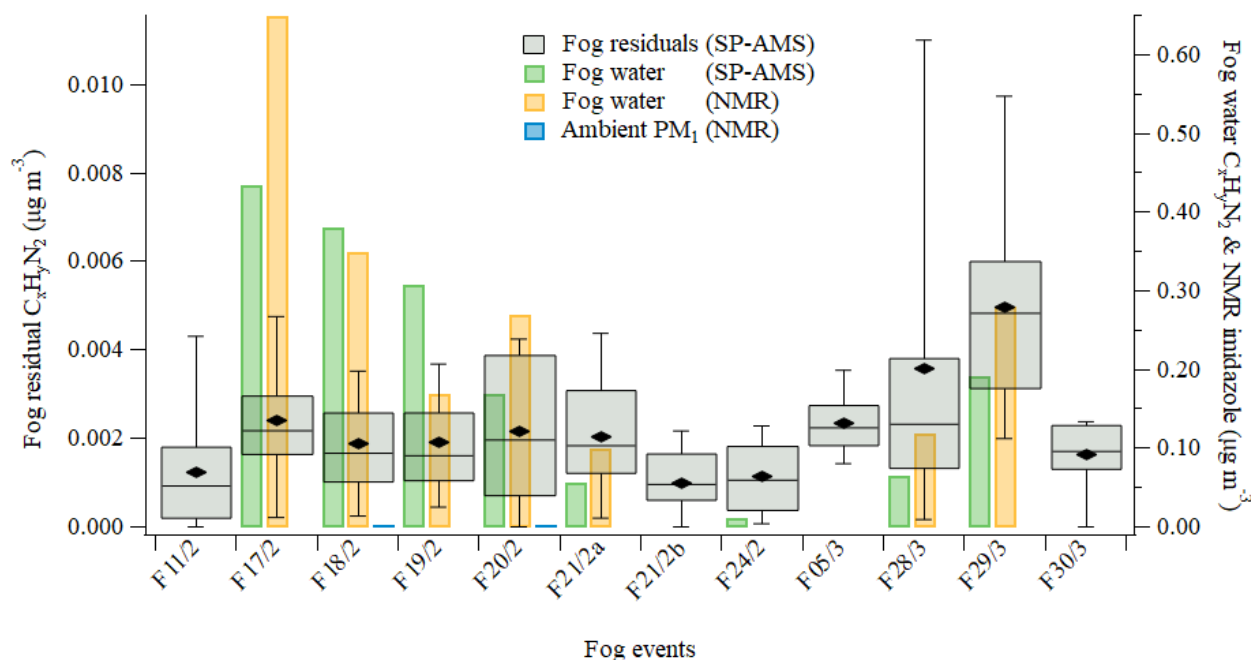
Figure 6. Mass concentration of $C_xH_yN_2^+$ measured by SP-AMS, and 1H-imidazole by NMR spectroscopy for each fog event. Fog resid-
ual $C_xH_yN_2^+$ (left y-axis) is represented by the boxes (75th and 25th percentile) and whiskers above and below the boxes (90th and 10th
percentile), the diamonds indicate the mean, and the lines indicate the median. The fog water $C_xH_yN_2^+$, together with fog water and PM_1
1H-imidazole (right y-axis).

4 Conclusions

Aqueous-phase processing of aerosol particles and fog chemistry was studied in the Po Valley during winter-time, as part of
the FAIRARI 2021/22 campaign. The sub-micron aerosol chemical characterization was carried out using one SP-AMS, for
the ambient aerosol and fog residuals, and one HR-TOF-AMS, for the interstitial aerosol. The ambient PM_1 concentration was
on average 13.5 ($\pm$ 9.1) μg m^{-3} throughout the campaign, which included 39% OA, 33% NO_3^-, 8% SO_4^{2-}, 12% NH_4^+, 1%
Cl^-, and 4% rBC. Compared to previous winter-time measurements at the site, the PM_1 mass was slightly lower, while still
being dominated by OA, although to a lesser degree.

During two pollution episodes, consisting of high relative humidity and high levels of pollution, several fog events were
captured. The sampling of the dried fog droplets (fog residuals) was done by applying a ground-based GCVI inlet. While the
chemical composition of the fog residuals was relatively similar over these periods, the ambient aerosol was NO_3^--dominated

in the first period, whereas OA dominated the ambient aerosol in the second period. This was likely due to the on average lower temperature and simultaneously higher RH, which allowed more gas-particle partitioning of especially inorganic compounds.

Fog water samples were collected and analyzed with an offline nebulizer setup, using the same SP-AMS. The fog water contained an unexpectedly large fraction of total OA, especially $C_xH_y^+$ ions, while the signal of more oxygenated $C_xH_yO_{>1}^+$ ions was lower. This stood out in comparison to the ambient aerosol and fog residuals, and resulted in lower than expected N:C and O:C ratios, not consistent with previous fog water studies. Similar to this study, previous fog/cloud studies found that the mass scavenging efficiency is lower for OA than e.g. NO_3^- and SO_4^{2-}, and that the cloud residual mass fraction of OA typically is lower than that of the ambient aerosol. Furthermore, the mass concentration of the OA families measured by the interstitial AMS and the SP-AMS agreed well during the non-fog periods. Thus, we hypothesize this discrepancy could be due to potentially different chemical composition in larger fog droplets, which were sampled well by the FWC, while the GCVI only samples fog droplets smaller than $40\,\mu m$ diameter.

A significant enhancement of ON was found in both fog residuals and fog water samples, which also proved to be highly correlated. The fog-enhanced ON consisted of several $C_xH_yN_1^+$ ions, likely originating from various amino compounds, while a few ions could be identified as primary and secondary amines. Notably, a good linear correlation with glyoxal fragments was found throughout the campaign (ambient r=0.80 and fog residuals r=0.84), suggesting a preferred partitioning of amines into the aqueous phase.

The $C_xH_yN_2^+$ ions, mainly present in the fog water, suggest formation of imidazole in the fog droplets. The related fragments linked to imidazole can from now on be used as tracer-fragments, confirmed by 1H-NMR spectroscopy. We hypothesize the reason they were less present in the fog residuals was that they were more concentrated in the large fog droplets, not sampled by the GCVI inlet. During the second fog intensive period, these $C_xH_yN_2^+$ ions were elevated in the fog residuals, and even persisted in the aerosol phase after fog dissipation, which shows the importance of fog processing from an air quality perspective. The results from this study improve our understanding on fog processing, and demonstrate that fogs and clouds are an important medium for aqueous production of certain nitrogen-containing organic aerosol in the atmosphere.

Data availability. All data, including HR-AMS mass spectra, will collectively be available at the Bolin Centre for Climate Research data base.

Author contributions. FM, PZ, IR, and CM designed the study. FM, AN, LH, YG, MP, MR, SD, PZ and CM collected the data at the SPC site. FM processed and analyzed the SP-AMS data. AN and PZ processed the GCVI data. MP processed and analyzed the 1H-NMR spectroscopy data. MR processed and analyzed the interstitial HR-TOF-AMS data. FM performed the overall analysis, data visualization, and wrote the paper with input from CM, IR, and PZ. All authors gave comments and suggestions on the paper.

Competing interests. Some authors are members of the editorial board of journal Atmospheric Chemistry and Physics.

Acknowledgements. Financial support from the European Union's Horizon 2020 research and innovation programme (project FORCeS under grant agreement No 821205, "NPF-PANDA" under grant agreement No. 895875), European Research Council (Consolidator grant INTE-GRATE No 865799), Knut and Alice Wallenberg Foundation (grant numbers 2021.0169 and 2021.0298) are gratefully acknowledged.
395 We thank Maurizio Busetto and David Hadden for their technical support in the field.

References

Bauer, S., Koch, D., Unger, N., Metzger, S., Shindell, D., and Streets, D.: Nitrate aerosols today and in 2030: a global simulation including aerosols and tropospheric ozone, Atmospheric Chemistry and Physics, 7, 5043–5059, 2007.

Cai, J., Sulo, J., Gu, Y., Holm, S., Cai, R., Thomas, S., Neuberger, A., Mattsson, F., Paglione, M., Decesari, S., et al.: Elucidating the mechanisms of atmospheric new particle formation in the highly polluted Po Valley, Italy, Atmospheric Chemistry and Physics, 24, 2423–2441, 2024.

Canagaratna, M., Jimenez, J., Kroll, J., Chen, Q., Kessler, S., Massoli, P., Hildebrandt Ruiz, L., Fortner, E., Williams, L., Wilson, K., et al.: Elemental ratio measurements of organic compounds using aerosol mass spectrometry: characterization, improved calibration, and implications, Atmospheric Chemistry and Physics, 15, 253–272, 2015.

Cape, J., Cornell, S., Jickells, T., and Nemitz, E.: Organic nitrogen in the atmosphere – Where does it come from? A review of sources and methods, Atmospheric Research, 102, 30–48, 2011.

Carbone, C., Decesari, S., Mircea, M., Giulianelli, L., Finessi, E., Rinaldi, M., Fuzzi, S., Marinoni, A., Duchi, R., Perrino, C., et al.: Size-resolved aerosol chemical composition over the Italian Peninsula during typical summer and winter conditions, Atmospheric Environment, 44, 5269–5278, 2010.

Chakraborty, A., Ervens, B., Gupta, T., and Tripathi, S. N.: Characterization of organic residues of size-resolved fog droplets and their atmospheric implications, Journal of Geophysical Research: Atmospheres, 121, 4317–4332, 2016.

Chen, X., Xie, M., Hays, M. D., Edgerton, E., Schwede, D., and Walker, J. T.: Characterization of organic nitrogen in aerosols at a forest site in the southern Appalachian Mountains, Atmospheric chemistry and physics, 18, 6829–6846, 2018.

De Haan, D. O., Corrigan, A. L., Smith, K. W., Stroik, D. R., Turley, J. J., Lee, F. E., Tolbert, M. A., Jimenez, J. L., Cordova, K. E., and Ferrell, G. R.: Secondary organic aerosol-forming reactions of glyoxal with amino acids, Environmental science & technology, 43, 2818–2824, 2009.

De Haan, D. O., Hawkins, L. N., Kononenko, J. A., Turley, J. J., Corrigan, A. L., Tolbert, M. A., and Jimenez, J. L.: Formation of nitrogen-containing oligomers by methylglyoxal and amines in simulated evaporating cloud droplets, Environmental science & technology, 45, 984–991, 2011.

DeCarlo, P. F., Kimmel, J. R., Trimborn, A., Northway, M. J., Jayne, J. T., Aiken, A. C., Gonin, M., Fuhrer, K., Horvath, T., Docherty, K. S., et al.: Field-deployable, high-resolution, time-of-flight aerosol mass spectrometer, Analytical chemistry, 78, 8281–8289, 2006.

Decesari, S., Paglione, M., Mazzanti, A., and Tagliavini, E.: NMR spectroscopic applications to atmospheric organic aerosol analysis–Part 1: A critical review of data source and analysis, potentialities and limitations, TrAC Trends in Analytical Chemistry, p. 117516, 2024.

Duplessis, P., Bhatia, S., Hartery, S., Wheeler, M. J., and Chang, R. Y.-W.: Microphysics of aerosol, fog and droplet residuals on the Canadian Atlantic coast, Atmospheric Research, 264, 105 859, 2021.

EEA: Air quality in Europe - 2020 report, https://doi.org/doi/10.2800/786656, 2020.

Ehrenhauser, F. S., Khadapkar, K., Wang, Y., Hutchings, J. W., Delhomme, O., Kommalapati, R. R., Herckes, P., Wornat, M. J., and Valsaraj, K. T.: Processing of atmospheric polycyclic aromatic hydrocarbons by fog in an urban environment, Journal of Environmental Monitoring, 14, 2566–2579, 2012.

Ervens, B.: Modeling the processing of aerosol and trace gases in clouds and fogs, Chemical reviews, 115, 4157–4198, 2015.

Ervens, B., Turpin, B., and Weber, R.: Secondary organic aerosol formation in cloud droplets and aqueous particles (aqSOA): a review of laboratory, field and model studies, Atmospheric Chemistry and Physics, 11, 11 069–11 102, 2011.

Facchini, M. C., Fuzzi, S., Zappoli, S., Andracchio, A., Gelencsér, A., Kiss, G., Krivácsy, Z., Mészáros, E., Hansson, H.-C., Alsberg, T., et al.: Partitioning of the organic aerosol component between fog droplets and interstitial air, Journal of Geophysical Research: Atmospheres, 104, 26 821–26 832, 1999.

Fountoukis, C. and Nenes, A.: ISORROPIA II: a computationally efficient thermodynamic equilibrium model for K^+–Ca^{2+}–Mg^{2+}–NH_4^+–Na^+–SO_4^{2-}–NO_3^-–Cl^-–H_2O aerosols, Atmospheric Chemistry and Physics, 7, 4639–4659, 2007.

Fuzzi, S., Orsi, G., Bonforte, G., Zardini, B., and Franchini, P. L.: An automated fog water collector suitable for deposition networks: Design, operation and field tests, Water, air, and soil pollution, 93, 383–394, 1997.

Galloway, M., Chhabra, P., Chan, A., Surratt, J., Flagan, R., Seinfeld, J., and Keutsch, F.: Glyoxal uptake on ammonium sulphate seed aerosol: reaction products and reversibility of uptake under dark and irradiated conditions, Atmospheric Chemistry and Physics, 9, 3331–3345, 2009.

Ge, X., Wexler, A. S., and Clegg, S. L.: Atmospheric amines – Part I. A review, Atmospheric Environment, 45, 524–546, 2011.

Ge, X., Zhang, Q., Sun, Y., Ruehl, C. R., and Setyan, A.: Effect of aqueous-phase processing on aerosol chemistry and size distributions in Fresno, California, during wintertime, Environmental Chemistry, 9, 221–235, 2012.

Ge, X., Sun, Y., Trousdell, J., Chen, M., and Zhang, Q.: Enhancing characterization of organic nitrogen components in aerosols and droplets using high-resolution aerosol mass spectrometry, Atmospheric Measurement Techniques, 17, 423–439, 2024.

Gilardoni, S., Massoli, P., Giulianelli, L., Rinaldi, M., Paglione, M., Pollini, F., Lanconelli, C., Poluzzi, V., Carbone, S., Hillamo, R., et al.: Fog scavenging of organic and inorganic aerosol in the Po Valley, Atmospheric Chemistry and Physics, 14, 6967–6981, 2014.

Gilardoni, S., Massoli, P., Paglione, M., Giulianelli, L., Carbone, C., Rinaldi, M., Decesari, S., Sandrini, S., Costabile, F., Gobbi, G. P., et al.: Direct observation of aqueous secondary organic aerosol from biomass-burning emissions, Proceedings of the National Academy of Sciences, 113, 10 013–10 018, 2016.

Giulianelli, L., Gilardoni, S., Tarozzi, L., Rinaldi, M., Decesari, S., Carbone, C., Facchini, M., and Fuzzi, S.: Fog occurrence and chemical composition in the Po valley over the last twenty years, Atmospheric Environment, 98, 394–401, 2014.

Goldstein, A. H. and Galbally, I. E.: Known and unexplored organic constituents in the Earth's atmosphere, Environmental science & technology, 41, 1514–1521, 2007.

Graeffe, F., Heikkinen, L., Garmash, O., Aijala, M., Allan, J., Feron, A., Cirtog, M., Petit, J.-E., Bonnaire, N., Lambe, A., et al.: Detecting and Characterizing Particulate Organic Nitrates with an Aerodyne Long-ToF Aerosol Mass Spectrometer, ACS Earth and Space Chemistry, 7, 230–242, 2022.

Hallquist, M., Wenger, J. C., Baltensperger, U., Rudich, Y., Simpson, D., Claeys, M., Dommen, J., Donahue, N., George, C., Goldstein, A., et al.: The formation, properties and impact of secondary organic aerosol: current and emerging issues, Atmospheric chemistry and physics, 9, 5155–5236, 2009.

Herrmann, H., Schaefer, T., Tilgner, A., Styler, S. A., Weller, C., Teich, M., and Otto, T.: Tropospheric aqueous-phase chemistry: kinetics, mechanisms, and its coupling to a changing gas phase, Chemical reviews, 115, 4259–4334, 2015.

Jia, X., Quan, J., Zheng, Z., Liu, X., Liu, Q., He, H., and Liu, Y.: Impacts of anthropogenic aerosols on fog in North China Plain, Journal of Geophysical Research: Atmospheres, 124, 252–265, 2019.

Jickells, T., Baker, A., Cape, J., Cornell, S., and Nemitz, E.: The cycling of organic nitrogen through the atmosphere, Philosophical Transactions of the Royal Society B: Biological Sciences, 368, 20130 115, 2013.

Jimenez, J. L., Canagaratna, M., Donahue, N., Prevot, A., Zhang, Q., Kroll, J. H., DeCarlo, P. F., Allan, J. D., Coe, H., Ng, N., et al.: Evolution of organic aerosols in the atmosphere, science, 326, 1525–1529, 2009.

Karlsson, L., Krejci, R., Koike, M., Ebell, K., and Zieger, P.: A long-term study of cloud residuals from low-level Arctic clouds, Atmospheric Chemistry and Physics, 21, 8933–8959, 2021.

Kim, H., Collier, S., Ge, X., Xu, J., Sun, Y., Jiang, W., Wang, Y., Herckes, P., and Zhang, Q.: Chemical processing of water-soluble species and formation of secondary organic aerosol in fogs, Atmospheric Environment, 200, 158–166, 2019.

475 Lampilahti, J., Manninen, H. E., Nieminen, T., Mirme, S., Ehn, M., Pullinen, I., Leino, K., Schobesberger, S., Kangasluoma, J., Kontkanen, J., et al.: Zeppelin-led study on the onset of new particle formation in the planetary boundary layer, Atmospheric chemistry and physics, 21, 12 649–12 663, 2021.

Laskin, A., Smith, J. S., and Laskin, J.: Molecular characterization of nitrogen-containing organic compounds in biomass burning aerosols using high-resolution mass spectrometry, Environmental science & technology, 43, 3764–3771, 2009.

480 Laskin, A., Laskin, J., and Nizkorodov, S. A.: Chemistry of atmospheric brown carbon, Chemical reviews, 115, 4335–4382, 2015.

Masson-Delmotte, V., Zhai, P., Pirani, A., Connors, S. L., Péan, C., Berger, S., Caud, N., Chen, Y., Goldfarb, L., Gomis, M., et al.: Climate change 2021: the physical science basis, Contribution of working group I to the sixth assessment report of the intergovernmental panel on climate change, 2, 2021.

Mazzoleni, L. R., Ehrmann, B. M., Shen, X., Marshall, A. G., and Collett Jr, J. L.: Water-soluble atmospheric organic matter in fog: ex-
485 act masses and chemical formula identification by ultrahigh-resolution Fourier transform ion cyclotron resonance mass spectrometry, Environmental science & technology, 44, 3690–3697, 2010.

Middlebrook, A. M., Bahreini, R., Jimenez, J. L., and Canagaratna, M. R.: Evaluation of composition-dependent collection efficiencies for the Aerodyne aerosol mass spectrometer using field data, Aerosol Science and Technology, 46, 258–271, 2012.

Montero-Martínez, G., Rinaldi, M., Gilardoni, S., Giulianelli, L., Paglione, M., Decesari, S., Fuzzi, S., and Facchini, M. C.: On the water-
490 soluble organic nitrogen concentration and mass size distribution during the fog season in the Po Valley, Italy, Science of the total environment, 485, 103–109, 2014.

Ng, N. L., Brown, S. S., Archibald, A. T., Atlas, E., Cohen, R. C., Crowley, J. N., Day, D. A., Donahue, N. M., Fry, J. L., Fuchs, H., et al.: Nitrate radicals and biogenic volatile organic compounds: oxidation, mechanisms, and organic aerosol, Atmospheric chemistry and physics, 17, 2103–2162, 2017.

495 Noone, K. J., Ogren, J. A., Hallberg, A., Heintzenberg, J., Strom, J., Hansson, H.-C., Svenningsson, B., Wiedensohler, A., Fuzzi, S., Facchini, M. C., et al.: Changes in aerosol size- and phase distributions due to physical and chemical processes in fog, Tellus B, 44, 489–504, 1992.

Onasch, T., Trimborn, A., Fortner, E., Jayne, J., Kok, G., Williams, L., Davidovits, P., and Worsnop, D.: Soot particle aerosol mass spectrom-
eter: development, validation, and initial application, Aerosol Science and Technology, 46, 804–817, 2012.

Paglione, M., Gilardoni, S., Rinaldi, M., Decesari, S., Zanca, N., Sandrini, S., Giulianelli, L., Bacco, D., Ferrari, S., Poluzzi, V., et al.: The
500 impact of biomass burning and aqueous-phase processing on air quality: a multi-year source apportionment study in the Po Valley, Italy, Atmospheric Chemistry and Physics, 20, 1233–1254, 2020.

Paglione, M., Decesari, S., Rinaldi, M., Tarozzi, L., Manarini, F., Gilardoni, S., Facchini, M. C., Fuzzi, S., Bacco, D., Trentini, A., et al.: Historical changes in seasonal aerosol acidity in the Po Valley (Italy) as inferred from fog water and aerosol measurements, Environmental science & technology, 55, 7307–7315, 2021.

505 Perrino, C., Catrambone, M., Dalla Torre, S., Rantica, E., Sargolini, T., and Canepari, S.: Seasonal variations in the chemical composition of particulate matter: a case study in the Po Valley. Part I: macro-components and mass closure, Environmental Science and Pollution Research, 21, 3999–4009, 2014.

Petzold, A. and Schönlinner, M.: Multi-angle absorption photometry—a new method for the measurement of aerosol light absorption and atmospheric black carbon, Journal of Aerosol Science, 35, 421–441, 2004.

510 Powelson, M. H., Espelien, B. M., Hawkins, L. N., Galloway, M. M., and De Haan, D. O.: Brown carbon formation by aqueous-phase carbonyl compound reactions with amines and ammonium sulfate, Environmental science & technology, 48, 985–993, 2014.

Rabaud, N. E., Ebeler, S. E., Ashbaugh, L. L., and Flocchini, R. G.: Characterization and quantification of odorous and non-odorous volatile organic compounds near a commercial dairy in California, Atmospheric Environment, 37, 933–940, 2003.

Rehbein, P. J., Jeong, C.-H., McGuire, M. L., Yao, X., Corbin, J. C., and Evans, G. J.: Cloud and fog processing enhanced gas-to-particle
515 partitioning of trimethylamine, Environmental Science & Technology, 45, 4346–4352, 2011.

Saarikoski, S., Carbone, S., Decesari, S., Giulianelli, L., Angelini, F., Canagaratna, M., Ng, N., Trimborn, A., Facchini, M., Fuzzi, S., et al.: Chemical characterization of springtime submicrometer aerosol in Po Valley, Italy, Atmospheric Chemistry and Physics, 12, 8401–8421, 2012.

Scotto, F., Bacco, D., Lasagni, S., Trentini, A., Poluzzi, V., and Vecchi, R.: A multi-year source apportionment of PM2. 5 at multiple sites in
520 the southern Po Valley (Italy), Atmospheric Pollution Research, 12, 101 192, 2021.

Seinfeld, J. H. and Pandis, S. N.: Atmospheric chemistry and physics: from air pollution to climate change, John Wiley & Sons, 2016.

Shingler, T., Dey, S., Sorooshian, A., Brechtel, F., Wang, Z., Metcalf, A., Coggon, M., Mülmenstädt, J., Russell, L., Jonsson, H., et al.: Characterisation and airborne deployment of a new counterflow virtual impactor inlet, Atmospheric Measurement Techniques, 5, 1259–1269, 2012.

525 Stephens, M., Turner, N., and Sandberg, J.: Particle identification by laser-induced incandescence in a solid-state laser cavity, Applied optics, 42, 3726–3736, 2003.

Sueper, D.: ToF-AMS Data Analysis Software Webpage, available at: http://cires1.colorado.edu/jimenez-group/wiki/index.php/ToF-AMS_ Analysis_Software (last access: 8 Feb 2024), 2024.

Sun, Y., Zhang, Q., Anastasio, C., and Sun, J.: Insights into secondary organic aerosol formed via aqueous-phase reactions of phenolic
530 compounds based on high resolution mass spectrometry, Atmospheric Chemistry and Physics, 10, 4809–4822, 2010.

Sun, Y.-L., Zhang, Q., Schwab, J., Demerjian, K., Chen, W.-N., Bae, M.-S., Hung, H.-M., Hogrefe, O., Frank, B., Rattigan, O., et al.: Characterization of the sources and processes of organic and inorganic aerosols in New York city with a high-resolution time-of-flight aerosol mass apectrometer, Atmospheric Chemistry and Physics, 11, 1581–1602, 2011.

Szopa, S., Naik, V., Adhikary, B., Artaxo, P., Berntsen, T., Collins, W. D., Fuzzi, S., Gallardo, L., Kiendler-Scharr, A., Klimont, Z., et al.:
535 Short-Lived Climate Forcers (Chapter 6), 2021.

Teich, M., van Pinxteren, D., Kecorius, S., Wang, Z., and Herrmann, H.: First quantification of imidazoles in ambient aerosol particles: potential photosensitizers, brown carbon constituents, and hazardous components, Environmental science & technology, 50, 1166–1173, 2016.

Timko, M. T., Yu, Z., Kroll, J., Jayne, J. T., Worsnop, D. R., Miake-Lye, R. C., Onasch, T. B., Liscinsky, D., Kirchstetter, T. W., Destaillats,
540 H., et al.: Sampling artifacts from conductive silicone tubing, Aerosol Science and Technology, 43, 855–865, 2009.

Vecchi, R., Piziali, F., Valli, G., Favaron, M., and Bernardoni, V.: Radon-based estimates of equivalent mixing layer heights: A long-term assessment, Atmospheric environment, 197, 150–158, 2019.

Youn, J.-S., Crosbie, E., Maudlin, L., Wang, Z., and Sorooshian, A.: Dimethylamine as a major alkyl amine species in particles and cloud water: Observations in semi-arid and coastal regions, Atmospheric Environment, 122, 250–258, 2015.

545   Yu, L., Smith, J., Laskin, A., Anastasio, C., Laskin, J., and Zhang, Q.: Chemical characterization of SOA formed from aqueous-phase
         reactions of phenols with the triplet excited state of carbonyl and hydroxyl radical, Atmospheric Chemistry and Physics, 14, 13 801–
         13 816, 2014.

       Zhang, G., Bi, X., Chan, L. Y., Li, L., Wang, X., Feng, J., Sheng, G., Fu, J., Li, M., and Zhou, Z.: Enhanced trimethylamine-containing
         particles during fog events detected by single particle aerosol mass spectrometry in urban Guangzhou, China, Atmospheric environment,
550   55, 121–126, 2012.

       Zhang, Q. and Anastasio, C.: Chemistry of fog waters in California's Central Valley—Part 3: Concentrations and speciation of organic and
         inorganic nitrogen, Atmospheric Environment, 35, 5629–5643, 2001.

       Zhang, Q., Jimenez, J. L., Canagaratna, M., Allan, J. D., Coe, H., Ulbrich, I., Alfarra, M., Takami, A., Middlebrook, A., Sun, Y., et al.:
         Ubiquity and dominance of oxygenated species in organic aerosols in anthropogenically-influenced Northern Hemisphere midlatitudes,
555   Geophysical research letters, 34, 2007.